Characterization of Titanium Effects on Very High Energy Electron (VHEE) Beams

El Mehdi Essaidi[1*], *Mustapha* Krim[1], *Abdessamad* Didi[1], *Meriem* Tantaoui[2], and *Othmane* Kaanouch[1]

[1]Hassan First University of Settat, High Institute of Health Sciences, Laboratory of Sciences and Health Technologies, BP 555, 26000, Settat, Morocco.

[2]Subatomic Research and Applications Team, Laboratory of the Physics of Condensed Matter (LPMC-ERSA), Faculty of Sciences Ben M'Sik, Hassan II University, BP 7955, Casablanca, Morocco

Abstract. Very High Energy Electron (VHEE) therapy is gaining attention as an innovative approach for treating deep-seated tumors, combining favorable dose deposition, sharp lateral penumbra, and compatibility with ultra-high dose rate (FLASH) delivery. A critical aspect of clinical translation is understanding how beamline components and high-density materials, such as patient implants or collimators, influence beam quality and secondary radiation production. In this work, we performed a comprehensive Monte Carlo investigation of titanium effects on collimated and magnetically focused VHEE beams using TOPAS/Geant4. A 10 × 10 cm², 150 MeV electron beam was directed into a water phantom containing a titanium insert at 5 cm depth. Phase-space planes were scored downstream of the insert to quantify electron, photon, positron, and neutron yields, energy spectra, angular distributions, and spatial fluence maps. Percentage depth–dose (PDD) curves were also evaluated. Titanium produced negligible energy degradation of primary electrons (<0.5% mean loss) but induced modest angular broadening, >70% photon yield enhancement via bremsstrahlung, and nearly two orders of magnitude increase in neutron production through photonuclear reactions near the giant dipole resonance. Focused beams demonstrated improved fluence recovery and maintained distal dose conformity. These results inform material selection, shielding design, and treatment planning for future VHEE radiotherapy systems.

1 Introduction

Radiotherapy is a cornerstone of cancer treatment, with approximately half of all cancer patients receiving radiation as part of their therapeutic regimen (Mohan and Grosshans, 2017 [1]). The fundamental goal of radiotherapy is to deliver a tumoricidal dose to the target volume while minimizing dose to surrounding healthy tissues and organs at risk (OARs). Advances such as three-dimensional conformal radiotherapy (3D-CRT), Intensity-Modulated Radiotherapy (IMRT), and Volumetric Modulated Arc Therapy (VMAT) have significantly improved the precision of dose delivery, reducing treatment-related toxicity (Li et al., 2020 [2]). However, for deep-seated tumors, conventional megavoltage photon beams are still challenged by dose deposition characteristics, including gradual build-up, broad

*Corresponding author: elmehdiessaidi@gmail.com

penumbra, and non-negligible exit dose, which can compromise dose conformity and spare critical structures (Paganetti et al., 2021 [3]).

Particle therapy with protons and heavier ions has emerged as a solution to some of these limitations. The Bragg peak allows for sharp dose fall-off beyond the target, leading to reduced normal tissue exposure (Graeff et al., 2023 [4]). Nevertheless, proton therapy facilities are expensive, require large gantries, and face challenges related to range uncertainties and secondary neutron production (Held et al., 2020 [5]; Wu and Fan, 2022 [6]). The cost and complexity of such infrastructures limit global accessibility, motivating the search for alternative modalities that can offer improved dose distributions with lower implementation barriers (Loap et al., 2021 [7]).
Very High Energy Electron (VHEE) therapy has recently gained renewed attention as a potential middle ground between conventional photon therapy and hadron therapy (DesRosiers et al., 2000 [8]; Bazalova-Carter et al., 2015 [9]). VHEE beams, in the 50–250 MeV energy range, can penetrate deep-seated tumors while retaining many of the advantageous characteristics of electron beams, including a relatively uniform dose deposition in the target volume and a sharp lateral penumbra due to reduced multiple scattering at higher energies. Monte Carlo studies have demonstrated that VHEE beams can achieve conformal dose distributions comparable to protons for many clinical cases, particularly when combined with intensity modulation or scanning beam techniques (Lagzda et al., 2020 [10]; Fisher et al., 2017 [11]). Additionally, VHEE systems are more compact and cost-effective compared to proton facilities, potentially enabling broader clinical adoption. Another unique advantage is their compatibility with ultra-high dose rate (FLASH) delivery, which has shown promising results in preclinical models for reducing normal tissue toxicity without compromising tumor control (Favaudon et al., 2014 [12]; Schuler et al., 2017 [13]).

However, the clinical translation of VHEE therapy requires a thorough understanding of how beam-shaping components and patient-related heterogeneities influence dose distribution and secondary particle production. High-density materials placed in the beam path, whether as part of beam collimation systems, patient-specific apertures, or orthopedic implants, can lead to increased production of bremsstrahlung photons and photonuclear neutrons (Zhao et al., 2020 [14]; Jia et al., 2015 [15]; Verburg and Seco, 2013 [16]). These secondary particles contribute to out-of-field dose and pose radioprotection challenges. Accurate modeling of these effects is crucial both for treatment planning and for shielding design of VHEE treatment rooms (Oancea et al., 2018 [17]).

Titanium is one of the most common materials encountered in radiotherapy workflows. Clinically, it is used in orthopedic implants, dental prostheses, and surgical clips. In accelerator and beamline design, titanium is used for collimators, scattering foils, and vacuum windows because of its favorable combination of strength, corrosion resistance, and relatively low atomic number compared to tungsten or lead (Brown and Lemons, 1996 [18]; Niinomi, 2008 [19]). Titanium's moderate Z offers a compromise between mechanical robustness and reduced bremsstrahlung production, but its impact on VHEE beams, particularly on particle spectra and secondary radiation yields, has not been thoroughly characterized in the literature.

Previous work has examined dosimetric characteristics of VHEE beams in water phantoms and compared them with protons and photons, but systematic investigations of how titanium modifies VHEE beam properties remain limited (Bazalova et al., 2007 [20]; Essaidi et al., 2025 [21]). Most studies have focused on depth–dose curves or clinical plan quality metrics, with little emphasis on phase-space characterization, spectral changes, angular distributions, and spatial fluence patterns in the presence of beamline materials.

The present study provides a systematic Monte Carlo characterization of titanium effects on Very High Energy Electron (VHEE) beam transport using TOPAS/Geant4. Both collimated and magnetically focused delivery configurations were simulated with and without a titanium insert positioned at a clinically relevant depth in a water phantom. Phase-space data were analyzed to extract electron, photon, positron, and neutron yields, along with their energy spectra, angular distributions, and spatial fluence maps. In addition, percentage depth–dose (PDD) curves were computed to quantify implant-induced perturbations in dose deposition. This comprehensive approach enables direct assessment of how titanium modifies primary electron fluence, enhances secondary photon and neutron production, and affects spatial dose conformity. The findings reported here have direct implications for the selection of collimator materials, optimization of beam-shaping strategies, shielding design, and treatment planning considerations in future VHEE radiotherapy systems.

2 Materials and Methods

2.1 Simulation Setup and Geometry

Monte Carlo simulations were carried out using TOPAS/Geant4 to model Very High Energy Electron (VHEE) beams with a nominal energy of 150 MeV. TOPAS provides a user-friendly interface to the GEANT4 toolkit and has been widely adopted for medical physics applications, including electron and proton beam modeling (Arce et al., 2021 [22]; Jarlskog and Paganetti, 2008 [23]). The simulation geometry consisted of a 30 × 30 × 30 cm^3 water phantom positioned at a source-to-surface distance (SSD) of 100 cm, consistent with standard setups used in recent VHEE investigations (Essaidi et al., 2025 [21]; Lagzda et al., 2020 [10]). A square electron field of 10 × 10 cm^2 was incident along the phantom's central axis (Z-axis).

To study the interaction of VHEE beams with high-density materials, a titanium insert (4 × 3 × 2 cm^3, density 4.48 g/cm^3) was placed at a depth of 5 cm below the entrance surface, mimicking clinically relevant metallic implants such as orthopedic prostheses and fixation devices (Brown and Lemons, 1996 [18]; Niinomi, 2008 [19]). The modeled insert material corresponded to the Ti-6Al-4V alloy (density = 4.48 g/cm^3), consisting of approximately 89.17 % Ti, 6.20 % Al, 4.00 % V, 0.30 % Fe, 0.20 % O, 0.08 % C, and 0.05 % N. Although a uniform titanium block was modeled for simplicity, patient implants vary in geometry and alloy composition (e.g., Ti-6Al-4V). These factors will be investigated to assess their impact on scattering and secondary radiation.

The phase-space scoring plane was positioned immediately downstream of the insert to record particle transport characteristics, following best practices for phase-space scoring in high-energy beam studies (Bazalova-Carter et al., 2015 [9]; Oancea et al., 2018 [17]).

Particle yields, energy spectra, angular distributions, and spatial coordinates were collected for electrons, photons, positrons, and neutrons. In addition, depth–dose distributions were scored within the water phantom to quantify the dosimetric impact of titanium, consistent with methods used in previous Monte Carlo dosimetry studies (Zhao et al., 2020 [14]; Jia et al., 2015 [15]). Figure 1 provides an overview of the simulation geometry, including beam field size, phantom dimensions, and titanium placement

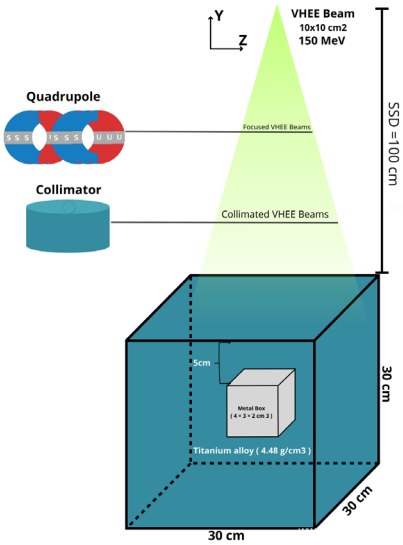

Fig. 1. Simulation setup showing VHEE beam delivery, water phantom, and titanium insert (4 × 3 × 2 cm^3 at 5 cm depth) for collimated and quadrupole-focused configurations.

2.2 Monte Carlo Modeling and Physics Settings

All simulations were performed using the TOPAS (Tool for Particle Simulation) platform (version 3.9), which provides a user-friendly interface to the GEANT4.10.7.p03 toolkit. GEANT4 is a widely validated C++ framework used for detailed modeling of particle interactions with matter and is considered a gold standard in medical physics research (Jarlskog and Paganetti, 2008 [23]). The physics list applied in this study was based on previously benchmarked configurations for radiotherapy applications [23,24], ensuring accurate representation of Very High Energy Electron (VHEE) transport and secondary particle production.

The selected physics models included multiple Coulomb scattering, energy loss by ionization, bremsstrahlung emission, electron–positron pair production, positron annihilation, and photonuclear reactions to account for neutron production. Neutron and proton transport were explicitly enabled to capture the contribution of secondary hadronic components, which, although of low probability, are clinically relevant for shielding and radioprotection assessments (Hall et al., 2016 [24]). The main processes and corresponding production thresholds are summarized in Table 1.

For each simulation, 10^6 primary electrons were generated to guarantee statistically robust results. A global range cut of 0.1 mm was adopted to ensure accurate step length control and spatial resolution without excessively increasing computational time. Energy cutoffs were set to allow full tracking of electrons, photons, neutrons, and positrons throughout the phantom. The resulting statistical uncertainty in the scored dose was kept below 2% in high-dose regions.

In this work, the primary focus was the characterization of titanium effects on VHEE beam quality. Phase-space planes were scored immediately downstream of the titanium insert and analyzed to extract particle yields, spectra, angular distributions, and fluence maps. Depth–dose distributions were calculated within the water phantom to quantify titanium-induced perturbations in energy deposition. This configuration allowed a systematic comparison between beams traversing titanium and reference beams in homogeneous water.

Table 1. Physics lists used in TOPAS simulations

Physics List	Description
g4em-standard_opt4	Electromagnetic interactions with precision settings
g4h-phy_QGSP_BERT_HP	High-precision hadronic inelastic and elastic physics using Bertini cascade and HP neutron models
g4h-elastic_HP	Elastic scattering of hadrons at low and high energies
g4ion-binarycascade	Inelastic interactions of light ions
g4em-extra	Photo-nuclear and gamma-nuclear processes
g4stopping	Energy loss and stopping power for charged particles
g4decay	Radioactive decay of unstable isotopes
g4radioactivedecay	Modeling of radioactive decay chains

3 Results and Discussion

3.1 Depth–Dose Analysis of VHEE Beams with Titanium

The percentage depth–dose (PDD) distributions for Very High Energy Electron (VHEE) beams in water, with and without titanium, are shown in Figure 2 (collimated delivery) and Figure 3 (magnetically focused delivery). In both scenarios, the titanium insert (4 × 3 × 2 cm^3) was positioned at a depth of 5 cm from the phantom surface, representing a clinically relevant situation where orthopedic prostheses or fixation plates are located close to the beam entrance.

For the collimated configuration, the presence of titanium caused noticeable perturbations in the buildup region and immediately downstream of the interface. Compared with the water-only reference, the titanium-modified PDD exhibited a localized reduction in dose of up to 8–10 %, primarily between 5 and 7 cm depth. This behavior reflects enhanced multiple Coulomb scattering and bremsstrahlung generation as electrons traverse the high-density insert, consistent with the findings of Jia et al. (2015) [15], Zhao et al. (2020) [14], and Bazalova et al. (2007) [20] in studies of high-Z heterogeneities. Importantly, beyond 10 cm depth, the curves gradually reconverged, confirming that the perturbation effect is spatially confined and does not significantly influence the distal dose fall-off (Verburg and Seco, 2013 [16]).

For the focused configuration, the introduction of titanium also produced a measurable reduction in entrance dose and a steeper buildup slope. Nevertheless, the location and amplitude of the focal peak (~15 cm depth) were essentially preserved, demonstrating that magnetic focusing largely compensates for lateral scatter and maintains beam convergence. The inset of Figure 3 highlights that, although a local dose dip is still present just after the titanium interface, the beam regains its fluence and matches the water reference at the focal depth. The observed mitigation effects were obtained under ideal beam stability. In realistic clinical scenarios, patient motion and magnetic field fluctuations could influence the degree of compensation, and future implementations should incorporate motion-management and active magnetic-field control systems. These results reinforce the robustness of focused VHEE delivery, showing that beam focusing can partially mitigate implant-induced perturbations and preserve distal dose conformity.

Overall, these findings demonstrate that titanium produces moderate but clinically relevant perturbations near the entrance region, which must be considered in treatment planning. The ability of VHEE beams to recover downstream of the heterogeneity, particularly under focused delivery, suggests that titanium implants may not compromise deep-target coverage if beam shaping and planning are optimized. These results are consistent with previous Monte Carlo studies by Bedri et al. (2025) [25], which reported that titanium implants cause significantly lower dose attenuation (−3.46 %) compared with Co-Cr-Mo (−19.26 %) and stainless steel (−11.8 %) under 150 MeV VHEE irradiation.

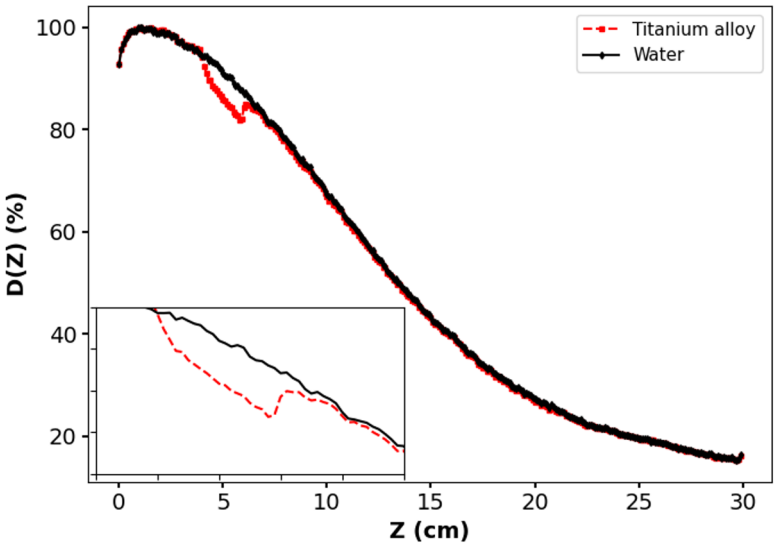

Fig. 2. PDD of VHEE beams in water and with titanium insert (collimated setup). Inset shows dose drop just after the implant.

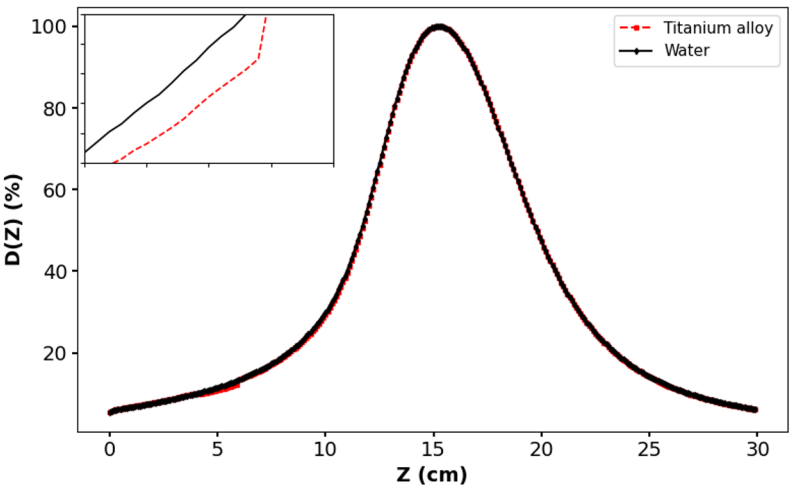

Fig. 3. PDD of VHEE beams in water and with titanium insert (focused setup). Inset highlights dose perturbation near the implant while maintaining focal peak alignment.

3.2 Particle Energy Spectra Analysis

The normalized energy spectra for primary and secondary particles are presented in Figure 4. The electron spectrum (Fig. 4a) shows a narrow peak near the nominal beam energy for all configurations, with minimal energy degradation following passage through the titanium insert. This observation is consistent with the Bethe–Bloch formalism, which predicts a

nearly constant stopping power for electrons in the hundreds-of-MeV range, resulting in limited energy loss per unit path length (Andreo et al., 2019 [26]).

In contrast, the photon spectrum (Fig. 4b) exhibits a broad bremsstrahlung tail extending across the entire energy range, with a higher photon yield in the presence of titanium. This is expected due to the bremsstrahlung cross-section scaling with approximately Z2, leading to enhanced photon production when the beam interacts with higher-Z materials (Bazalova-Carter et al., 2015 [9]). Titanium increased photon yield by approximately 70 % and neutron yield by two orders of magnitude. While absolute doses remain low, such enhancements necessitate careful shielding evaluation and consideration of out-of-field dose. The overall photon fluence was slightly reduced in the focused configuration compared with the collimated case, indicating that focusing concentrates the primary electron fluence and reduces off-axis scatter that contributes to photon background.

The neutron spectrum (Fig. 4c) demonstrates that titanium increases neutron yield, particularly in the epithermal and fast energy range, attributable to photonuclear reactions such as (γ,n) near the giant dipole resonance region (Oancea et al., 2018 [17]; Stasica et al., 2023 [27]). Although the absolute neutron count remains low, this highlights the importance of including neutron transport in dosimetric and radioprotection assessments.

Positron spectra (Fig. 4d) confirm the presence of electron–positron pair production at high energies, with similar distributions across configurations. Focused beams slightly reduce the number of positrons relative to collimated ones, likely due to improved beam confinement and lower off-axis photon fluence.

Overall, the spectral analysis demonstrates that titanium primarily enhances secondary photon and neutron production while exerting minimal impact on the primary electron energy spectrum. This emphasizes the need for accurate modeling of secondary radiation when metallic implants are present, particularly in scenarios where out-of-field dose or shielding is of clinical concern.

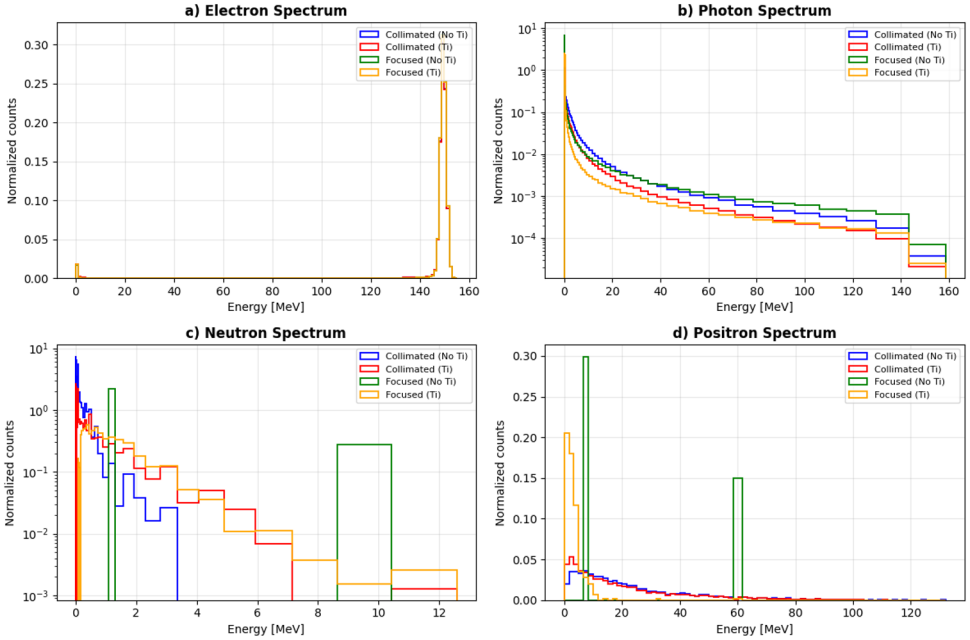

Fig. 4. Normalized energy spectra for electrons (a), photons (b), neutrons (c), and positrons (d) for collimated and focused VHEE beams, with and without titanium inserts.

3.3 Angular Distributions of Primary and Secondary Particles

The angular distributions shown in Figure 5 provide insight into the scattering and secondary particle production mechanisms within the phantom. The electron angular distribution (Fig. 5a) is strongly forward-peaked for all configurations, with most electrons remaining within a few degrees of the beam axis. This behavior is consistent with Molière's theory of multiple Coulomb scattering, which predicts a narrow angular spread for high-energy electrons, with θ_0 scaling inversely with momentum (Bazalova-Carter et al., 2015 [9]). The presence of the titanium insert causes a slight broadening of the forward peak, reflecting increased multiple scattering in the higher-Z medium.

The photon angular distribution (Fig. 5b) exhibits a broader spread, extending to large angles due to bremsstrahlung emission. Titanium increases the overall photon fluence and slightly flattens the angular distribution, consistent with enhanced Z2-dependent bremsstrahlung production (Lagzda et al., 2020 [10]). Focused beams show a slightly reduced wide-angle photon component, demonstrating that magnetic focusing confines the primary electron trajectories and reduces off-axis photon generation (Fisher et al., 2017 [11]).

Neutron angular distributions (Fig. 5c) are more isotropic, as expected for photonuclear reactions, but their intensity is noticeably higher in the presence of titanium. This is attributable to (γ,n) reactions occurring near the giant dipole resonance, which produce neutrons with a nearly isotropic emission pattern (Oancea et al., 2018 [17]).

Finally, positron angular distributions (Fig. 5d) are relatively broad, arising from pair production events induced by high-energy bremsstrahlung photons. Titanium slightly increases the positron yield but does not significantly change the angular shape.

Overall, these results highlight that titanium increases wide-angle scatter and secondary particle production, but magnetic focusing partially mitigates these effects by preserving forward-directed electron fluence. These findings support the potential benefit of focusing systems in improving dose conformity and minimizing off-axis dose spread in clinical VHEE applications (Lagzda et al., 2020 [10]; Fisher et al., 2017 [11]).

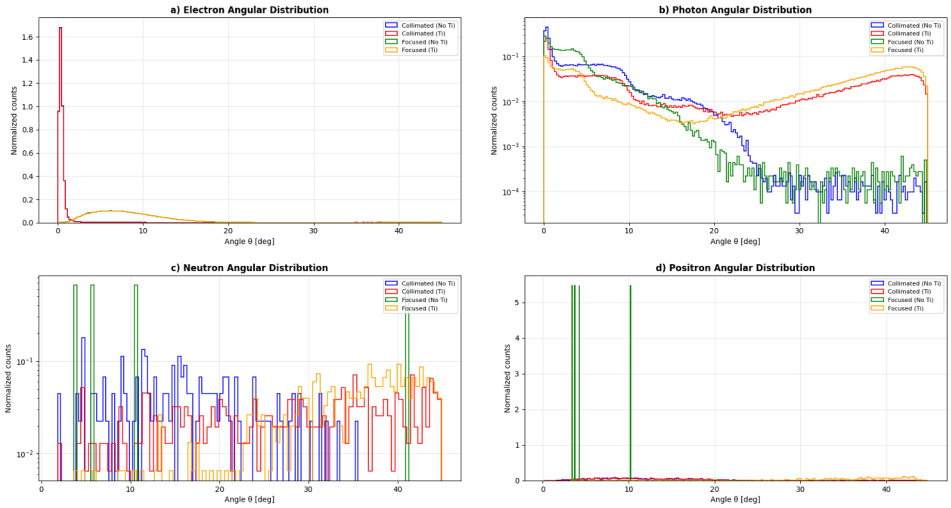

Fig. 5. Angular distributions of electrons (a), photons (b), neutrons (c), and positrons (d) for collimated and focused VHEE beams, with and without titanium inserts.

3.4 2D Fluence Maps of Primary and Secondary Particles

The fluence maps presented in Figure 6 provide a spatial visualization of particle transport and secondary production across the transverse (X–Y) plane at the scoring plane downstream of the phantom entrance.

For electrons (Figs. 6a–d), both collimated and focused beams exhibit a symmetric, Gaussian-like fluence profile centered on the beam axis, with focused beams showing a visibly narrower distribution, consistent with the magnetic quadrupole focusing effect (Lagzda et al., 2020 [10]). The presence of titanium slightly reduces the central fluence, reflecting attenuation and scattering within the insert, but the overall beam symmetry is maintained.

Photon fluence maps (Figs. 6e–h) display a more diffuse spatial distribution, with a noticeable halo extending beyond the primary electron field due to bremsstrahlung production. Titanium inserts significantly increase the off-axis photon fluence, particularly in the focused case (Fig. 6h), as the higher-Z material enhances bremsstrahlung generation

(∝Z2) and produces more wide-angle photons (Bazalova-Carter et al., 2015 [9]). This is clinically relevant because it may contribute to out-of-field dose, though the absolute magnitude remains small compared to the electron fluence.

Neutron fluence maps (Figs. 6i–l) show sparse but distinct events distributed across the scoring plane, confirming low-probability photonuclear reactions. Titanium notably increases neutron fluence (Fig. 6j and 6l), consistent with the increased (γ,n) cross-section in high-Z materials near the giant dipole resonance (Oancea et al., 2018 [17]). Focused beams tend to confine neutron production closer to the beam axis, which may reduce unintended dose to lateral structures.

Overall, these fluence map results highlight that titanium primarily affects secondary radiation production (photons and neutrons) rather than significantly distorting the primary electron spatial profile. Importantly, magnetic focusing enhances central beam confinement, which may help mitigate implant-induced dose perturbations and improve target coverage in clinical VHEE treatments (Lagzda et al., 2020 [10]; Bazalova-Carter et al., 2015 [9]).

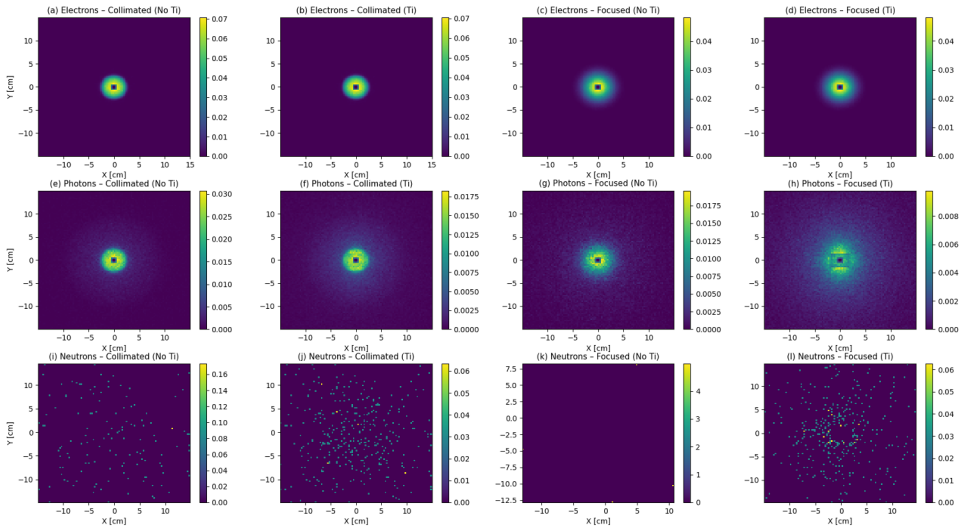

Fig. 6. Two-dimensional fluence maps of electrons (a–d), photons (e–h), and neutrons (i–l) for collimated and focused VHEE beams, with and without titanium inserts.

4 Conclusion

This study systematically characterized the effects of titanium on Very High Energy Electron (VHEE) beams using detailed Monte Carlo simulations in TOPAS/Geant4. Phase-space

analyses, spectral distributions, angular spreads, fluence maps, and depth–dose curves were evaluated for beams with and without titanium under both collimated and focused delivery configurations.

The results demonstrated that titanium introduces only a minimal reduction in primary electron mean energy (<0.5%) and a slight spectral broadening, confirming that the overall beam quality is largely preserved. In contrast, titanium significantly increases secondary photon production, leading to spectral softening dominated by low-energy bremsstrahlung, and produces a notable rise in neutron yield with spectral hardening due to photonuclear reactions. Focused delivery was shown to partially mitigate scattering-induced perturbations, preserving distal dose coverage even in the presence of titanium.

These findings provide quantitative evidence that titanium implants have a localized dosimetric impact, primarily confined to the buildup and near-field regions, while leaving the distal dose profile largely unaffected. The study highlights the importance of accurate modeling of secondary radiation and supports the use of titanium as a clinically favorable material for implants and collimator components in VHEE therapy. Future work should investigate patient-specific geometries and perform experimental validation to further refine treatment planning strategies and shielding requirements for upcoming VHEE clinical applications.

References

1. R. Mohan, D. Grosshans, *Adv. Drug Deliv. Rev.* **109**, 26 (2017). https://doi.org/10.1016/j.addr.2016.11.006
2. X. Li, A. Lee, M.A. Cohen, E.J. Sherman, N.Y. Lee, *Oral Oncol.* **110**, 104879 (2020). https://doi.org/10.1016/j.oraloncology.2020.104879
3. H. Paganetti, C. Beltran, S. Both, L. Dong, J. Flanz, K. Furutani, C. Grassberger, D.R. Grosshans, A.C. Knopf, *et al.*, *Phys. Med. Biol.* **66**, 05RM01 (2021).
4. C. Graeff, L. Volz, M. Durante, *Prog. Part. Nucl. Phys.* **131**, 104046 (2023). https://doi.org/10.1016/j.ppnp.2023.104046
5. K.D. Held, A.J. Lomax, E.G.C. Troost, *Br. J. Radiol.* **93**, 20209001 (2020). https://doi.org/10.1259/bjr.20209001
6. Y.Y. Wu, K.H. Fan, *Br. J. Radiol.* **95**, 20220294 (2022).
7. P. Loap, A. Mirandola, L. De Marzi, R. Dendale, A. Iannalfi, V. Vitolo, A. Barcellini, A.R. Filippi, B.A. Jereczek-Fossa, *et al.*, *Cancers* **13**, 3746 (2021). https://doi.org/10.3390/cancers13153746
8. C. DesRosiers, V. Moskvin, A.F. Bielajew, L. Papiez, *Phys. Med. Biol.* **45**, 1781 (2000). https://doi.org/10.1088/0031-9155/45/7/306
9. M. Bazalova-Carter, *et al.*, *Med. Phys.* **42**, 2615 (2015).

10. A. Lagzda, D. Angal-Kalinin, J. Jones, A. Aitkenhead, K.J. Kirkby, R. MacKay, M. van Herk, W. Farabolini, S. Zeeshan, R.M. Jones, *Nucl. Instrum. Methods Phys. Res. B* **482**, 70 (2020). https://doi.org/10.1016/j.nimb.2020.09.014

11. C.M. Fisher, *et al.*, *Phys. Med. Biol.* **62**, 4631 (2017).

12. V. Favaudon, *et al.*, *Sci. Transl. Med.* **6**, 245ra93 (2014). https://doi.org/10.1126/scitranslmed.3008973

13. E. Schuler, S. Trovati, G. King, B.W. Loo Jr., P.G. Maxim, E.A. Blakely, *et al.*, *Int. J. Radiat. Oncol. Biol. Phys.* **97**, 195 (2017). https://doi.org/10.1016/j.ijrobp.2016.10.030

14. L. Zhao, V.M. Moskvin, C.W. Cheng, I.J. Das, *Biomed. Phys. Eng. Express* **6**,

15. Y. Jia, L. Zhao, C.W. Cheng, M.W. McDonald, I.J. Das, *J. Appl. Clin. Med. Phys.* **16**, 333 (2015).

16. J.M. Verburg, J. Seco, *Med. Phys.* **40**, 071727 (2013).

17. C. Oancea, *et al.*, *Phys. Med. Biol.* **63**, 215020 (2018).

18. S.A. Brown, J.E. Lemons, *Medical Applications of Titanium and Its Alloys: The Material and Biological Issues* (ASTM International, West Conshohocken, PA, 1996). https://doi.org/10.1520/STP1176-EB

19. M. Niinomi, *J. Mech. Behav. Biomed. Mater.* **1**, 30 (2008). https://doi.org/10.1016/j.jmbbm.2007.07.001

20. M. Bazalova, *et al.*, *Phys. Med. Biol.* **52**, 123 (2007). https://doi.org/10.1088/0031-9155/52/4/001

21. E.M. Essaidi, M. Krim, O. Kaanouch, M. Tantaoui, M.R. Mesradi, D. Abdessamad, D. Benchekroun, *Atom Indones.* **50**, 1599 (2025).

22. P. Arce, *et al.*, *Med. Phys.* **48**, 19 (2021). https://doi.org/10.1002/mp.14658

23. C.Z. Jarlskog, H. Paganetti, *et al.*, *IEEE Trans. Nucl. Sci.* **55**, 1018 (2008). https://doi.org/10.1109/TNS.2008.922816

24. D.C. Hall, A. Makarova, *et al.*, *Phys. Med. Biol.* **61**, N1 (2016). https://doi.org/10.1088/0031-9155/61/1/N1

25. N.K. Bedri, M. Smetana, L. Janousek, *Impact of metallic implants on dose distribution in radiotherapy with electrons, photons, protons, and very-high-energy beams*, *Appl. Sci.* **15**, 4536 (2025). https://doi.org/10.3390/app15094536

26. P. Andreo, *et al.*, *Med. Phys.* **46**, 517 (2019). https://doi.org/10.1002/mp.13223

27. P. Stasica, *et al.*, *Phys. Med. Biol.* **68**, 104001 (2023).